Analytica Chimica Acta 1135 (2020) 123–131

Contents lists available at ScienceDirect

Analytica Chimica Acta

journal homepage: www.elsevier.com/locate/aca

Fe-MOFs as signal probes coupling with DNA tetrahedral nanostructures for construction of ratiometric electrochemical aptasensor

Fa-Ting Xie , Xiao-Lan Zhao , Kuan-Neng Chi , Tong Yang , Rong Hu **, Yun-Hui Yang *

College of Chemistry and Chemical Engineering, Yunnan Normal University, Kunming, Yunnan, 650500, PR China

HIGHLIGHTS

- A ratiometric electrochemical aptasensor is proposed for the detection of thrombin.
- The accessibility of target molecules and loading amounts of signal tags was increased own to DNA nanotetrahedron.
- Fe-MOFs as signal probe and the electrolyte solution as an inner reference probe.
- The ratiometric biosensor owns a strong ability to eliminate the disturbance.

GRAPHICAL ABSTRACT

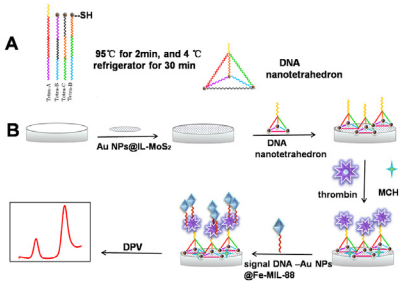

ARTICLE INFO

Article history:
Received 13 May 2020
Received in revised form
2 August 2020
Accepted 4 August 2020
Available online 22 August 2020

Keywords:
DNA nanotetrahedron
Thrombin
Ratiometric
Fe-MOFs
Aptasensor

ABSTRACT

A ratiometric electrochemical aptasensor is proposed for the detection of thrombin. In the sensor, the iron metal-organic frameworks (Fe MOFs)-labeled aptamer as signal tags was used as signal probe (SP), and the electrolyte solution $[Fe(CN)_6]^{3-/4-}$ was utilized as an inner reference probe (IR). In the presence of thrombin, the signal of Fe-MOFs can be detected. Meanwhile, the signal of $[Fe(CN)_6]^{3-/4-}_{-IR}$ almost remains stable. Accordingly, thrombin concentration can be monitored with the ratio response of $I_{Fe\text{-}MOFs\text{-}SP}/I^{3-/4-}_{[Fe(CN)6]\text{-}IR}$. The proposed ratiometric biosensor owns a strong ability to eliminate the disturbance that arises from different DNA loading densities, environmental impact and instrumental efficiency. DNA nanotetrahedron (NTH) with three-dimensional (3D) scaffold can effectively eliminate nonspecific adsorption of DNA and protein. The accessibility of target molecules and loading amounts of signal substances could be increased because of the enhanced mechanical rigidity of well-designed 3D NTH. Thus, detection reproducibility and sensitivity can be further improved. Moreover, the biosensor only requires conjugation with one electroactive substance. The modification procedure can be greatly simplified. The biosensor owns high sensitivity with the detection limit of 59.6 fM. We expect that it will emerge as a generalized ratiometric sensor that may be useful for detecting target analytes.

1. Introduction

Electrochemical biosensors have attracted widespread attention due to their simple instrumentation, high sensitivity, and easy operation [1–3]. Specially for electrochemical DNA biosensors, such

* Corresponding author.
** Corresponding author.
E-mail addresses: hudierong_168@163.com (R. Hu), yyhui2002@aliyun.com (Y.-H. Yang).

https://doi.org/10.1016/j.aca.2020.08.007
0003-2670/

biosensors have been used widely in various fields, such as environmental analysis, food processing, and medical diagnosis [2–5]. Unfortunately, they suffer easily from nonspecific adsorption, environmental factor and instrumental influence [6]. Generally speaking, introducing nanomaterials, such as DNA nanoparticles, on the surface of an electrode surface has commonly been used. The DNA nanotetrahedron (NTH) that is assembled using four single-stranded nucleic acids via one-step thermal denaturation has a stable structure [7,8]. NTH with three-dimensional (3D) scaffold easily functions with different chemical biomolecules [9], promoting effectively recognition of target [10]. Moreover, NTH can accurately locate the direction of a probe, reducing nonspecific adsorption of DNA and protein on an electrode interface [10–12]. However, the traditional DNA NTH biosensor usually use one signal input. Instrumental efficiency, and environmental conditions could affect the sensor's reproducibility. Therefore, developing a novel electrochemical biosensor is highly desirable.

In recent years, the ratiometric method has became an intelligent choice to improve the practical application of sensing system. The electroactive materials act as an inner reference probe (IR), and the ratio response between the signal probe (SP) and IR substance was utilized for a built-in correction [5,6,13,14]. Thus, the impact that arises from different DNA loading densities, temperature variation and nontarget-induced DNA dissociation can be reduced, providing more accurate signals through the sensor's self-referencing capability [5,6]. Currently, there are two working types of common ratiometric electrochemical DNA sensors. The first type immobilizes IR molecules at an electrode. Xiang et al. designed a dual signal hairpin DNA-based ratiometric strategy for the detection of mucin 1 [5]. Ellington et al. developed reagentless, ratiometric electrochemical DNA sensors for the detection of single nucleotide polymorphism (SNP) [6]. Two signal tags was usually required to label with nucleic acid. One was used as IR, the other was employed as SP. Commonly, ferrocene and methylene blue are utilized as signal tags for ratiometric DNA electrochemical sensors. The second type adds IR molecules to electrolyte solution. Compared to the first type, only one electroactive substance is required to conjugate with detection probes, such as nucleic acid. Thus, the second type is more appropriate for constructing ratiometric electrochemical biosensors because of their simplicity.

Metal-organic frameworks (MOFs) materials are consist of metal ions and organic linkers [15,16]. MOFs have tunable porosities, functional surfaces, and bulk conjugated backbones [17]. Because of their unique properties, MOFs have been extensively utilized in the fields of biosensing, drug delivery, and electric batteries [18–20]. For example, in our previous report, Cu MOFs were used as electrochemical signal tags [21]. Samples that contained large quantities of ions could offer high electrochemical signals. More interesting, Au-MOFs as a signal unit exhibited high signal amplification compared with other signal tags. These results motivate us to search more MOFs-based signal substances. It was found that Fe-MIL-88 can be used as a signal probe. In this work, more emphases are placed on the construction of novel, simple and signal-amplified electrochemical ratiometric DNA biosensors, in which Fe-MIL-88 was used as the signal probe and the electrolyte solution $K_3Fe(CN)_4/K_4Fe(CN)_6$ was used as an IR substance. Also, the Fe-MIL conjugation step with nucleic acid is uncomplicated since metal nanoparticles can be easily incorporated.

Thrombin is a protease that play an important part in the body's coagulation system [22]. The activity and concentration of thrombin can be used as an indicator of the coagulation mechanism [23]. Thrombin is closely related to physiological and pathological processes, for instance, inflammation, wound healing, and blood coagulation [24,25]. Aptamers are single-stranded RNA or DNA oligonucleotides, and they have the advantage that they combine a range of proteins and cells specifically and effectively [26–28]. Compared with antibodies, aptamers are more stable and adaptable and have more flexible modification [29]. Accordingly, developing a novel aptamer-based electrochemical ratiometric sensor (aptasensor) for highly sensitive, and selective quantification of thrombin is desirable.

In this paper, an electrochemical ratiometric aptasensor which owns strong ability to eliminate the disturbance of nonspecific adsorption, environmental change and instrumental efficiency is proposed for the quantification of thrombin (Fig. 1). Herein, the electrolyte solution $[Fe(CN)_6]^{3-/4-}$ was used as an IR probe, and Fe-MOFs-labeled aptamer was used as an SP probe. In contrast with the conventional ratiometric aptasensor, this sandwich-structure DNA aptasensor only requires conjugation with one electroactive substance. The modification procedure can be greatly simplified. Also, the electrolyte solution (IR molecules) is more stable than the DNA-labeled electroactive substance. Thus, random errors can be greatly reduced. Moreover, DNA NTH effectively eliminates nonspecific adsorption of DNA and protein, and detection accuracy is improved. Introducing an aminated ionic liquid (IL-NH_2) helps to stabilize MoS_2 via electrostatic repulsion. The proposed Au NPs@IL-MoS_2 which has large specific surface areas and good electroconductibility was used as a sensing interface to further improve detection sensitivity. Due to the aforementioned superiority, this ratiometric aptasensor achieves high reproducibility, accuracy, stability, and sensitivity. It is expected that this universal ratiometric sensor may be useful for detecting of other target analytes via according aptamer changes.

2. Experimental section

2.1. Experimental reagent and apparatus

6-Mercaptohexanol (MCH, 97%), thrombin, bovine serum albumin (BSA), C-reactive protein (CRP), alpha-fetoprotein (AFP), human chorionic gonadotropin (HCG), chitosan (CHIT), 1-(3-dimethylaminopropyl)-3-ethylcarbodiimideHydrochloride (EDC), Phosphate buffer saline (PBS, 0.01 mol/L phosphate, 0.138 mol/L NaCl, pH 7.4) and *N*-hydr oxysuccinimide (NHC) were purchased from Sigma (USA). Chloroauric acid ($HAuCl_4 \cdot 4H_2O$) was purchased from Sinopharm Chemical Reagent Co, Ltd. (Shanghai, China). MoS_2, 2-aminoterephthalic acid and trisodium citrate were acquired from Shanghai Aladdin Biochemical Technology Co, Ltd. (Shanghai, China). The DNA samples used in this study were obtained from Shanghai Sangon Biotechnology Co, Ltd. (Shanghai, China). The sequences of all of the oligonucleotides are given in Table S1. All of the other reagents were analytical reagent grade and used directly.

A CHI650E-electrochemical workstation used in this work and was purchased from Shanghai Chenhua Instrument Company (Shanghai, China). Transmission electron microscopy (TEM) was conducted using a JEM-200 (JEOL, Japan). X-ray photoelectron spectroscopy (XPS) measurement performed with a K-Alpha + X-spectrometer (Thermo Fisher Scientific, USA). X-ray diffraction (XRD) was determined using a TTRIII diffractometer (Nippon science Co, Japan).

2.2. Synthesis of DNA NTH materials

The purchased Tetra-A, Tetra-B, Tetra-C, and Tetra-D chains were added to a certain amount of Tris acetate buffer (20 mM, pH 8.0 containing 50 mM $MgCl_2$). Then, the four DNA chains were mixed equivalently in buffer, heated at 95 °C for 2 min, and then immediately deposited at 4 °C for 30 min. The synthesized DNA NTH was mixed in a 1:1 ratio with buffer; then, the mixture was

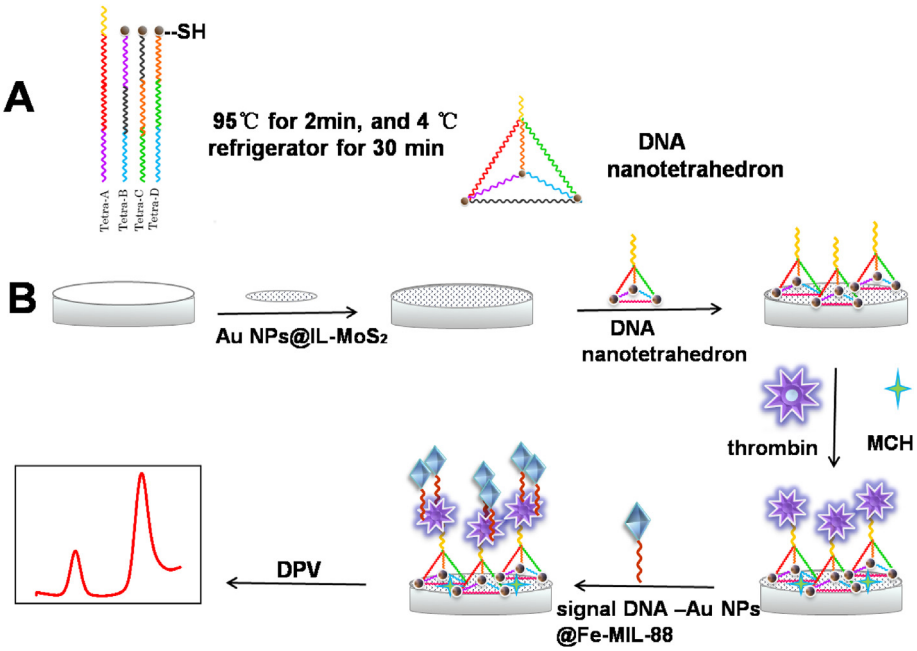

Fig. 1. Schematic illustration of the ratiometric electrochemical sensor.

diluted to 2.5 μM DNA nanotetrahedron [30].

2.3. Preparation of gold nanoparticles (Au NPs)

Au NPs were prepared via citrate reduction of tetrachloroauric acid according to the reported literature [31]. First, 500 μL of 1 mM $HAuCl_4 \cdot 4H_2O$ solution was heated under stirring. After boiling, 1.75 mL of 1.0% trisodium citrate was directly added into the above refluxing solution. The mixture was boiled for a period of time until the solution color turned to wine red. The gold nanoparticles were deposited at 4 °C for use.

2.4. Preparation of Au NPs@ Fe-MIL-88 hybrids

Fe-MIL-88 was slightly modified via previously reported methods [32]. For hydrothermal synthesis, 0.378 g of 2-aminoterephthalic acid and 0.561 g of $FeCl_3 \cdot 6H_2O$ were dissolved in 45 mL of dimethylformamide (DMF). Acetic acid (5 mL) was then added and heated at 120 °C for 4 h under stirring. After cooling to room temperature, the particles were collected by centrifugation (8000 rpm) and washed with DMF and absolute ethanol. Finally, the remaining solid was dried under a vacuum drying oven at 60 °C for overnight.

For the preparation of Au NPs@Fe-MIL-88 hybrids, 50 mg of Fe-MIL-88 powder was dispersed in 25 mL of sterilized water. Under vigorous stirring, Au NPs (25 mL) were slowly added. After 24 h, the Au NPs@Fe-MIL-88 material was washed with sterile water three times, and then dried.

2.5. Synthesis of Au NPs@IL-MoS_2 hybrids

A mixture of IL-NH_2 (10 g) and MoS_2 (25 mg) was dispersed in 50 mL water, and then 0.05 g of KOH was added. The solution was homogenized for half an hour. Then, the mixtures were heated and stirred at 80 °C for 24 h. After centrifugation (6000 rpm), IL-MoS_2 was washed 3 times with distilled water and anhydrous ethanol, and then dried.

Au NPs (20 mL) were slowly added to 20 mL of IL-MoS_2 solution (1 mg/mL) under vigorous stirring for 24 h. The mixtures were then rinsed with absolute ethanol and distilled water via centrifugation at 6000 rpm.

2.6. Au NPs@ Fe-MIL-88 labeled signal probe DNA

Au NPs@Fe-MIL-88 (10 mg) was dissolved in 500 μL H_2O. 200 μL of NHS (100 mM) and 200 μL of EDC (400 mM) were next added to the above mixture under stirring for 30 min. After centrifugation, the precipitates were scattered in 200 μL of distilled water. Streptavidin (200 μL, 0.5 mg/L) was then added to this mixed solution for 4 h at 4 °C. DNA1 (250 μL, 10 μM) was then added for 2 h at 4 °C. Under the help of NHS/EDC, the amino groups of Au NPs@Fe-MIL-88 and the carboxyl groups of streptavidin were combined. Afterwards, 1 mL of 1 mM mercaptoethanol (MCH) was added into the aforementioned mixture and shaken at 4 °C for 1 h. The white precipitate was centrifugated (12,000 rpm) and rinsed with PBS. Finally, the DNA-labeled Au NPs@Fe-MIL-88 was dispersed in 500 μL of sterilized water and deposited at 4 °C in a refrigerator for use.

2.7. Measurement procedure

Glassy carbon (GC) electrodes were polished using a previously reported method [33]. First, 10 μL of 1 mg/mL Au NPs@IL-MoS_2 solution was coated onto the electrode. After drying, 10 μL of 2.5 μM DNA NTH was added to obtain a sequential aptamer monolayer, and this was kept overnight at 37 °C. The improved electrodes were then permeated in 1 mM MCH for 10 min at 37 °C to block nonspecific binding sites. The modified GC electrodes were then dropped with 10 μL of thrombin for 1 h. Then, 10 μL of DNA-modified Au NPs@ Fe-MIL-88 was added for 1 h at 37 °C.

In the experiment, three electrodes were used to form a three-electrode system. GC electrode were utilized to as the working electrode, and a platinum electrode and a calomel electrode were the auxiliary electrode and the reference electrode, respectively. The sensor was detected using differential pulse voltammetry (DPV) in PBS containing 0.2 mM $K_3[Fe(CN)_6]/K_4[Fe(CN)_6]$.

3. Results and dicussion

3.1. Characterization

First, transmission electron microscopy (TEM) was used to investigate the morphology of the Au NPs@Fe-MIL-88 composite. As seen in Fig. 2A, the synthesized Fe-MIL-88 nanomaterial has an irregular octahedral structure with particle size of 200 nm, and this is similar to the literature report [34]. Also, gold nanoparticles are uniformly loaded on Fe-MIL-88 (Fig. 2B). XRD was utilized to characterize the structure of synthesized Fe-MIL-88 material. As seen in Fig. 2C, there is a strong peak near 10° and a slightly weak peak near 20°. Compared to the standard spectrum, the obtained results are consistent with the literature [34]. The surface survey XPS analysis of Fe-MIL-88 was demonstrated in Fig. 2D. The result displays the existence of C, O, N and Fe elements, revealing the successful synthesis of the composites (Fig. 2D). The spectrum of C 1s (Fig. S1) can be divided into two peaks that appear at C—N (288.3 eV) and C—C (284.6 eV) [35]. The spectrum of O 1s can be analyzed one peak at C═O (530.7 eV) (Fig. S2) [36]. The N 1s has three peaks (Fig. S3), which are attributed to N_{2C} (398.8 eV), N_{3C} (400.5 eV) and NH_X (399 0.0 eV) [37]. The Fe 2p XPS spectrum of the catalyst is fitted into three peaks, as shown in Fig. 2E. The peaks occur at 711.2 eV, 716.2 eV and 724.5 eV that are consistent with Fe^{3+} $2P_{3/2}$ [38]. UV spectrophotometry was then performed to further confirm the successful preparation of the Au NPs@Fe-MIL-88 composite. In Fig. 2F, a characteristic absorption peak at 520 nm was shown in curve a, which is the absorption spectra of gold nanoparticles. Curve b represents the absorption spectra of Fe-MIL-88. The absorption peak at 258 nm was detected. In curve c, there are two absorption peaks at 258 nm and 520 nm. The above-mentioned results explained the successful synthesis of Au NPs@Fe-MIL-88.

TEM was used to observe the morphology of Au NPs@IL-MoS_2. As seen in Fig. 3. MoS_2 nanosheets have a morphology of thin folded layers (Fig. 3 A). Fig. 3B shows that gold nanoparticles were loaded on MoS_2 and had a two-dimensional (2D) sheet structure. The dispersion of MoS_2 after amine-terminated IL-NH_2 loaded was shown in Fig. 3C. MoS_2 is more uniformly dispersed in ionic liquids than it is in water, and this indicates that IL-NH_2 helps to stabilize MoS_2. Meanwhile, MoS_2, IL-MoS_2, and Au NPs@IL-MoS_2 are characterized by Fourier transform infrared spectroscopy (FTIR), and the results are shown in Fig. 3D. For single MoS_2 (a), the peak that appears at 465 cm^{-1} is attributed to the Mo—S bond; furthermore, peaks at 1386 cm^{-1} and 1626 cm^{-1} are related to characteristic peaks of MoS_2 nanosheets [39]. For IL-MoS_2 (b), the doublet at 2844 cm^{-1} and 2915 cm^{-1} corresponds to symmetric Vs(CH_2) and asymmetric Vs(CH_2) of IL-NH_2 units which are adsorbed to the MoS_2 nanometer layer [40]. In addition, the CH_3 (N) stretch, CH_2 (N) stretch, and ring plane asymmetric stretch caused by the imidazole ring of IL are observed near 1200 cm^{-1} [40]. After Au NPs loaded on the surface of IL-MoS_2, the peaks were almost unchanged (c). These observations further confirm IL-NH_2 was attached to the MoS_2 nonmaterial.

DNA NTH was constructed by hybridization of four strands of DNA (Tetra A, B, C, and D). The formation of NTH was verified by agarose gel electrophoresis. As seen in Fig. 3E, Tetra A was single DNA, which has the lowest molecular weight. The fastest mobility appeared in the gel (lane 1). The complexity of spatial mass and increased mass hampered DNA movement. Thus, the migration rate of the bands of the BC hybrid and BCD hybrid chains were lower than that of Tetra A (lane 2 and lane 3). When Tetra A, B, C, and D are incubated together, a band was stuck in the wells (lane 4, 5), and this resulted from the formation of large molecular weights of DNA NTH. The difference in position indicates the successful synthesis of tetrahedral DNA nanomaterials. TEM was then carried out to further verify the successful formation of NTH. As seen in Fig. 3F, NTH has a circular structure with a uniform diameter [10]. From the above results, one can see that NTH was successfully synthesized.

3.2. Experimental principle

The principle of the ratiometric sensor is based on the ratios of the Fe-MOFs signal labeled with the thrombin aptamer and the electrochemical signals of $[Fe(CN)_6]^{3-/4-}$ in the detecting buffer. The electrolyte solution $[Fe(CN)_6]^{3-/4}$ was used as an IR probe, and Fe-MOFs-labeled aptamer was used as an SP probe. Introducing IL-NH_2 helps to stabilize MoS_2 via electrostatic repulsion. The proposed AuNPs@IL-MoS_2 hybrid, which has good electrical conductivity (Fig. S4), was used as a sensing interface. Then, the thiol (HS)-labeled DNA NTH was combined to sensing interface via the Au—S bond. In the presence of thrombin, the signal of Fe-MOFs was detected. Meanwhile, $[Fe(CN)_6]^{3-/4-}$ almost remains stable. Accordingly, the thrombin concentration can be monitored as a ratio response $I_{Fe\text{-}MOFs\text{-}SP}/I^{3-/4-}_{[Fe(CN)6]\text{-}IR}$.

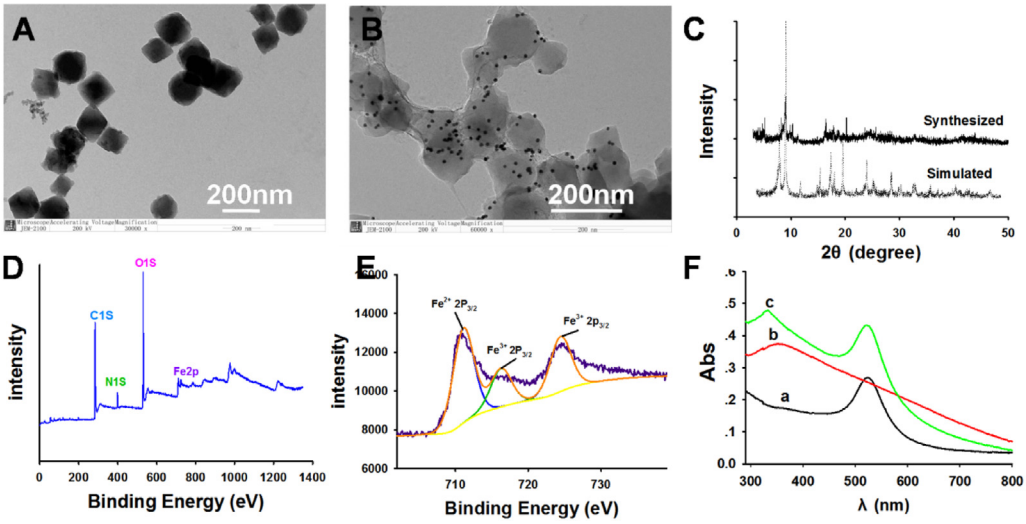

Fig. 2. TEM image of Fe-MIL-88 (A) and Au NPs@Fe-MIL-88 composite (B); (C) XRD of Fe-MIL-88; (D) Full XPS of Fe-MIL-88; (E) Fe 2p from Fe-MIL-88; (F) The UV vis spectra of (a) Au nanoparticles, (b) Fe-MIL-88 and (c) Au NPs@Fe-MIL-88 composite, respectively.

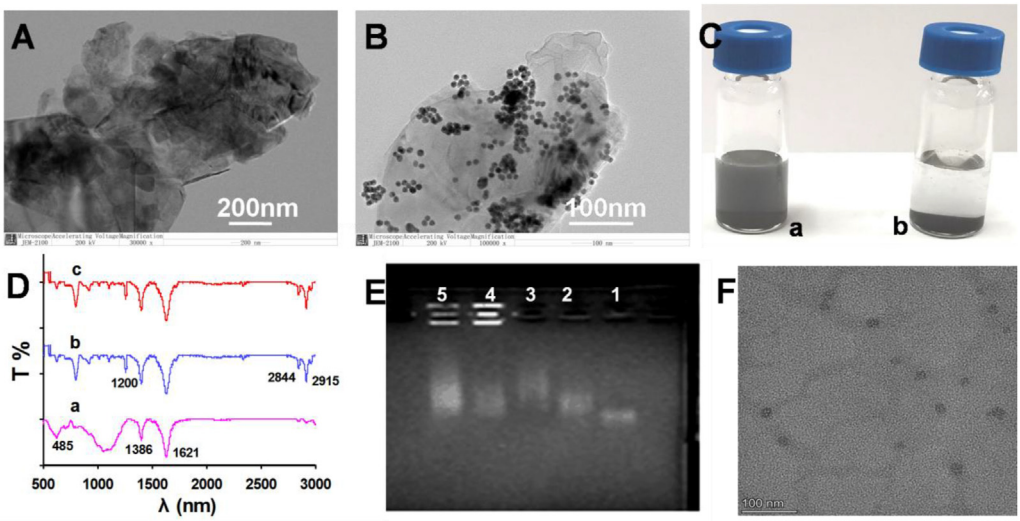

Fig. 3. TEM image of MoS_2 (A) and Au NPs@IL-MoS_2 composite (B); (C) The stability change of Au NPs@MoS_2 before (right) and after (left) adding IL-NH_2; (D) FTIR of MoS_2 (a), IL-MoS_2 (b) and Au NPs@IL-MoS_2 composite (c); (E) Gel electrophoresis image of Tetra A (lane 1), Tetra A-B (lane 2), Tetra A-B-C (lane 3), DNA NTH (lane 4, high DNA concentration), DNA NTH (lane 5, low DNA concentration); (F) TEM image of the NTH.

NTH with 3D scaffold could effectively reduce nonspecific adsorption of DNA and protein on the electrode interface. Therefore, our proposed sensor has the following distinguishing features: (1) The selectivity and reproducibility of biosensor is greatly improved because of the use of DNA NTH. (2) In contrast to traditional stem-loop or linear DNA probe, the accessibility of target molecules and loading amounts of signal substances could be increased [8], because of the enhanced mechanical rigidity of well-designed 3D NTH. Thus, the proposed biosensor exhibits excellent sensitivity. (3) The ratio response $I_{Fe\text{-}MOFs\text{-}SP}/I^{3-/4-}_{[Fe(CN)6]\text{-}IR}$ of this designed electrochemical sandwich-structure DNA biosensor does not result from adjusting the distance between two signal probes. The signal changes come from target binging of the sensing interface. This favors elimination of disturbances from the sensing electrode, and this can increase the accuracy of sensor. (4) Compared with the conventional ratiometric DNA aptasensor, this biosensor only requires conjugation with one electroactive substance. Thus, the procedure for the signal probe modification can be greatly simplified. Also, the electrolyte solution is more stable compared to the DNA-labeled electroactive substance. Therefore, our proposed ratiometric sensor is wished to own high stability, reproducibility, selectivity, and sensitivity.

3.3. Stability of the biosensor

To confirm that the stability and accuracy of the ratiometric electrochemical probe are higher than those of the non-ratiometric sensors, the stability of the ratiometric sensor was assessed. Ten electrodes with 30 individual measurements was used to collection the data, and the corresponding results are shown in Fig. 4. Fig. 4A displays DPV curves from three different electrodes. The current ratio between Fe-MOFs and $[Fe(CN)_6]^{3-/4}$ was almost the same on each GC electrode surface. As shown in Fig. 4B, similar to the classic electrochemical aptasensor, the current response of the non-proportional sensor in 30 individual tests demonstrated wide variation with an average of 14.4481 μA, and the relative standard deviation (RSD) is 18.3%. However, in our ratiometric electrochemical aptamer, the variation was significantly reduced. The RSD in 30 tests was calculated to be 4.38% with an average of 4.5066 (Fig. 4C). The obtained results indicate that the ratiometric method is more reliable, reproducible and stable than the non-ratiometric approach (Fig. 4D). The ratiometric sensor reduces background interference and random errors and obtains more accurate data. Consequently, the proposed ratiometric strategy is more accurate.

3.4. Characterization of the modified electrode

The preparation process of the modified electrode is characterized by electrochemical impedance spectroscopy (EIS) and cyclic voltammetry (CV). EIS can be utilized to monitor the surface modification and step-by-step construction of sensors. Changes in electron transfer resistance (Ret) are markedly connected to different electrode modifications. As seen in Fig. 5A, the bare electrode shows only a straight line (curve a, Ret = 40 Ω). When Au NPs@IL-MoS_2 was deposited onto the surface of the GC, a small semicircle diameter is observed (curve b, Ret = 80 Ω). The diameter of the semicircle distinctly increased after adding NTH on the electrode interface (curve c, Ret = 1000 Ω), because the presence of DNA NTH inhibited the electron transfer. The assembly of MCH led to a distinct increase in Ret (curve d, Ret = 1400 Ω). The Ret enhanced dramatically after assembling with thrombin (curve e, Ret = 1600 Ω). Thrombin is a biological macromolecule and has no electrical conductivity; this leads to increasement of the Ret value. When the signal probe DNA1-labeled Au NPs@Fe-MIL-88 specifically binds to the modified electrode, the Ret further increased (curve f, Ret = 1900 Ω).

The peak currents in CV results can also reveal electron transfer of $[Fe(CN)_6]^{3-/4-}$ on the surface of electrodes [5]. As seen in Fig. 5B, the bare GC electrode shows a redox peak with a good peak shape (curve a). When Au NPs@IL-MoS_2 was immobilized onto the cleaned electrode, the redox peak currents almost unchanged (curve b), showing high conductivity of these materials. Self-assembly of DNA NTH on the modified electrode then led to a decrease in the redox peak current (curve c), and this is attributed to the repulsion effect between negatively charged DNA NTH and $[Fe(CN)_6]^{3-/4-}$. MCH was then self-assembled, and after blocking remaining active sites, the redox peak current was decreased (curve d). When thrombin was added, a further decrease in the redox peak current was detected (curve e). When the signal probe signal DNA-Au NPs@Fe-MIL-88 specifically binds to modified electrode, it

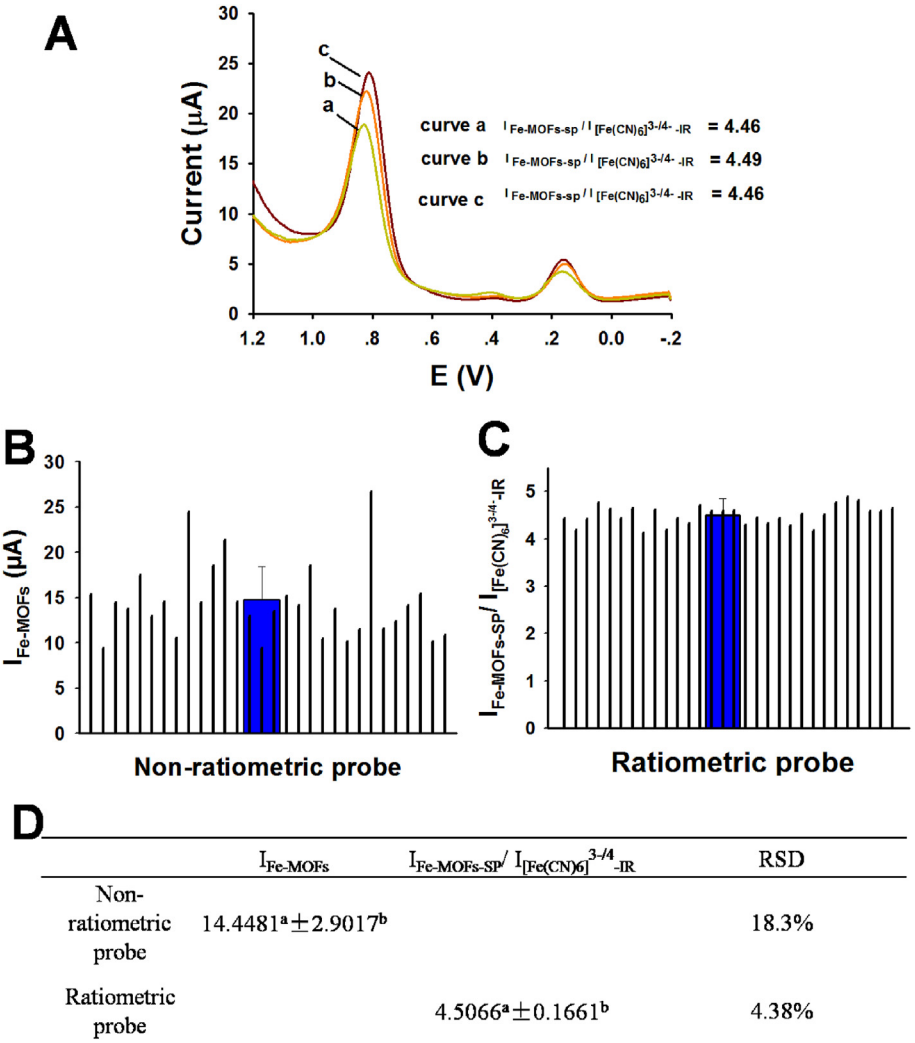

D

	$I_{Fe\text{-}MOFs}$	$I_{Fe\text{-}MOFs\text{-}SP}/I_{[Fe(CN)_6]^{3-/4-}\text{-}IR}$	RSD
Non-ratiometric probe	14.4481[a]±2.9017[b]		18.3%
Ratiometric probe		4.5066[a]±0.1661[b]	4.38%

Fig. 4. Comparison between ratiometric and non-ratiometric aptasensor. Typical DPV curves scanned after thrombin binding onto three different electrodes (A). Reproducibility of the non-ratiometric aptasensor (B), and ratiometric aptasensor (C). The black histogram stands for the response of 30 individual tests. The blue error bars and the black error bars in the blue histograms represent average values and the RSD of 30 measurements, respectively. $I_{Fe\text{-}MoFs\text{-}SP}$ stands for the currents response of 30 tests at 0.8 V after target binding. $I_{Fe\text{-}MoFs\text{-}SP}/I^{3-/4-}_{[Fe(CN)6]\text{-}IR}$ means the ratio response of 30 measurements. (D) The aforementioned data for proposed ratiometric and non-ratiometric probe. [a] Mean value of 30 determinations. [b] Standard deviation. (For interpretation of the references to color in this figure legend, the reader is referred to the Web version of this article.)

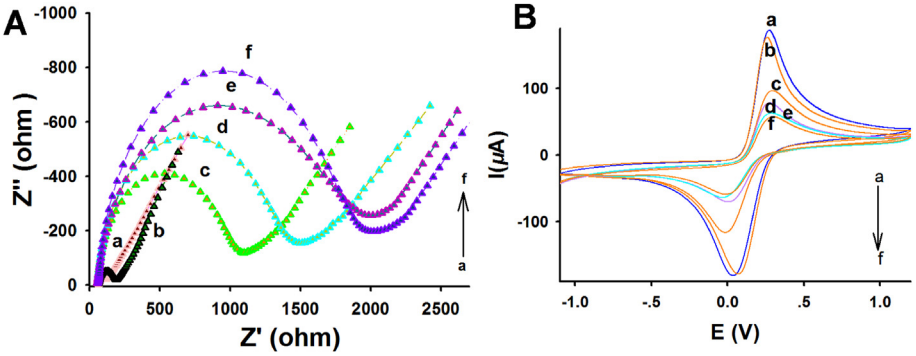

Fig. 5. Electrochemical impedance spectroscopy (A) and cyclic voltammetry (B) by using different modified electrodes (a: bare GC; b: Au NPs@IL-MoS_2/GC; c: NTH/Au NPs@IL-MoS_2/GC; d: MCH/NTH/Au NPs@IL-MoS_2/GC; e: thrombin/MCH/NTH/Au NPs@IL-MoS_2/GC; f: DNA1-Au NPs@Fe-MIL-88/thrombin/MCH/NTH/Au NPs@IL-MoS_2/GC). All tests were carried out in 10 mM $[Fe(CN)_6]^{3-}/[Fe(CN)_6]^{4-}$ containing 0.2 M KCl.

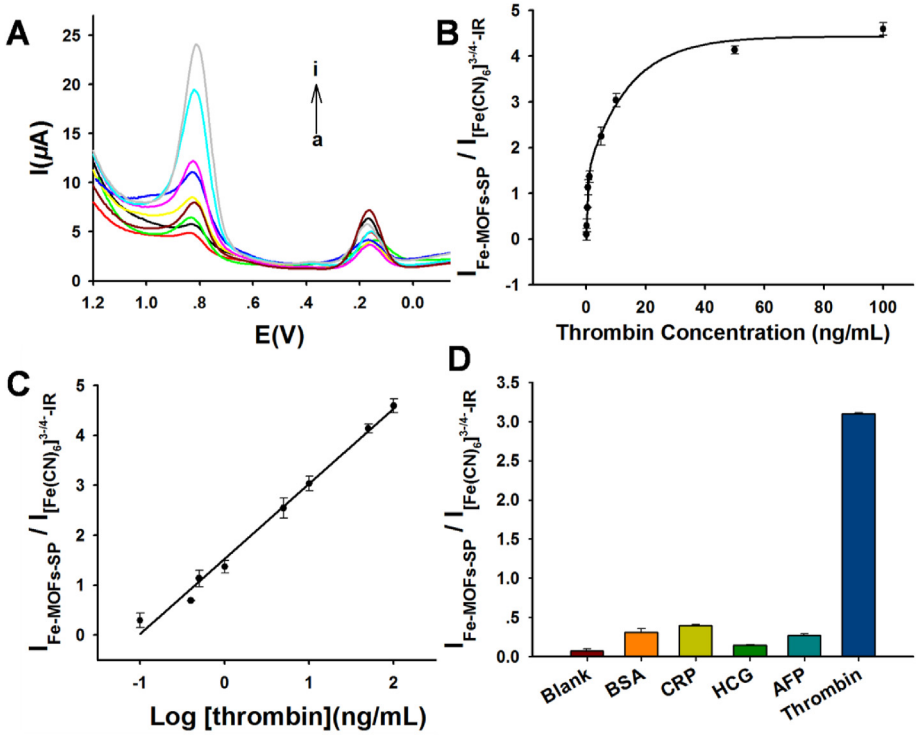

Fig. 6. (a) Typical DPV curves of the sensor in response to thrombin of varying concentrations. a: 0 ng/mL, b: 0.1 ng/mL, c: 0.4 ng/mL, d: 0.5 ng/mL, e: 1 ng/mL, f: 5 ng/mL, g: 10 ng/mL, h: 50 ng/mL, i: 100 ng/mL. (b) The current ratio enhancement with the increase of the thrombin concentration. (c) Relationship of the ratio response with the logarithm of the target concentration. (d) The selectivity of the biosensor.

hinders electron transfer, and the lowest redox peak current is observed (curve f).

3.5. Optimization of conditions

The concentration of $[Fe(CN)_6]^{3-/4-}$ can affect the current response of the sensor. Therefore, the influence of this concentration was detected. As seen in Fig. S5, when the $[Fe(CN)_6]^{3-/4-}$ consistence was gradually increased from 0.2 to 1 mM, the value of the ratio gradually decreased. Therefore, the optimal concentration for the experiment is 0.2 mM.

The pH of the PBS buffer can have an effect on the response current of Fe-MOFs. Thus, the pH of the detecting buffer was studied to determine the optimum performance. As seen in Fig. S6, the current response increased when the pH of the buffer increased. The maximum response was at a pH of 6.5, then it decreased with increasing pH from 7.0 to 8.5. Thus, a pH of 6.5 was selected for further experiments.

The amount of Au NPs in the hybridization of Au NPs@Fe-MIL-88 was also optimized. As seen in Fig. S7, when the volume of Au NPs was increased from 10 mL to 100 mL, the distribution of Au NPs on the surface of Fe MOFs was gradually enhanced. However, the EIS results shown that the Ret enhanced dramatically after the volume of Au NPs increased (Fig. S8). The volume of Au NPs with 25 mL could provide the minimum Ret value, which means the best conductivity for them. And the CV results were identical with the EIS. Therefore, the volume of Au NPs with 25 mL was used to preparation of Au NPs@ Fe-MIL-88 hybrids in the experiment.

3.6. Analytical performance

The prepared ratiometric sensor was then employed to detect different concentrations of thrombin to verify that the proposed sensor can be used for quantifying analyte. Fig. 6A shows the relationship between DPV responses of the proposed ratiometric aptasensor and target thrombin concentrations. When the concentration of thrombin increased, the peak current of Fe-MOFs-$_{SP}$ at +0.8 V gradually increased, whereas DPV responses of $[Fe(CN)_6]^{3-/4-}$$_{-IR}$ at +0.2 V did not change much. Therefore, the ratio response $I_{Fe\text{-}MoFs\text{-}SP}/I^{3-/4-}_{[Fe(CN)6]\text{-}IR}$ gradually increased with an enhance of thrombin concentration (Fig. 6B). Fig. 6C exhibits the linear curve of the ratiometric aptasensor. A good linear relationship between

Table 1
Analytical Performance of correlative methods for thrombin detection.

Sensing material	Liner ranger	Detection limit	Reference
hollow Au–CeO_2	0.5 pM-30 nM	0.25 pM	[41]
Gold Nanoparticles	0.1 nM–15 nM	0.1 nM	[42]
three-stranded DNA complexes	5 pM-1 nM	1.7 pM	[43]
nanofibrous	50 pM-5 nM	1.0 pM	[44]
NIR-emissive quantum dots poly adenine-gold nanoparticles	0.1–100 nM	34 pM	[45]
	0.1 pM-10 nM	35 fM	[46]
Fe-MIL-88	0.298–29.8 pM	59.6 fM	This work

Table 2
Recovery of thrombin in 10 fold-diluted human serum samples.

Sample	Added (ng/mL)	Found (ng/mL) n = 3	Average Found (ng/mL)	RSD (%)	Recovery (%)	Average Recovery (%)
1	5.000	5.073	5.027	0.797	101.4	100.04
		5.011			100.2	
		4.998			99.96	
2	10.00	10.05	10.04	0.664	100.5	
		10.10			101.0	
		9.968			99.68	
3	50.00	50.00	49.59	0.86	100.0	
		49.15			98.30	
		49.64			99.28	

the logarithm of thrombin concentration and the ratio response $I_{Fe\text{-}MoFs\text{-}SP}/I^{3-/4-}_{[Fe(CN)6]\text{-}IR}$ ranging from 0.1 ng/mL to 100 ng/mL (0.298 pM–29.8 pM) was obtained. The obtained linear equation is: $I_{Fe\text{-}MOFs\text{-}SP}/I^{3-/4-}_{[Fe(CN)6]\text{-}IR} = 1.5024\ \lg C + 1.5291$. The limit of detection (LOD) was calculated to 20 pg/mL (59.6 fM) at signal-to-noise ratio of 3. Due to the aforementioned distinguishing features, the sensitivity of the biosensor is better compared with some previous reported correlative work for thrombin (see Table 1) [41–46].

Selectivity is the significant factor for a biosensor. Thus, BSA, CRP, AFP, and HCG were selected as disruptors and were used to investigate specificity. As seen in Fig. 6D, although the concentration of interfering substances (50 ng/mL) is greater than that of thrombin (10 ng/mL), their response current ratio is much smaller than the response current ratio of the target. This result indicates that the proposed ratio sensor has good selectivity and can be used for detecting thrombin. Hence, this sensor provides a basis for the practical application of ratio sensors.

3.7. Sensor recovery

To verify that our proposed aptasensor can be used for real sample detection, the content of thrombin in human serum was determined. Blood samples were spiked with thrombin at different concentrations and were detected. Each concentration was measured 3 times in parallel, and the corresponding results are listed in Table 2. The average recovery of thrombin at a concentration of 5, 10, and 50 ng/mL was 100.04%. These results indicate that our proposed biosensor can be used for real sample detection.

4. Conclusions

A ratiometric electrochemical aptasensor was proposed for detecting thrombin. An internal reference probe ($[Fe(CN)_6]^{3-/4-}{}_{IR}$) was combined with a signal probe (Fe-MOFs-$_{SP}$) to form a complete dual-signal sandwich DNA biosensor. In contrast to non-proportional sensors, the proposed electrochemical ratiometric aptasensor demonstrates higher stability, reproducibility, and accuracy. In this paper, four DNA sequences were annealed to obtain DNA NTH with rich molecular modification sites. The DNA NTH end-modifies the thiol group and is easily assembled on the electrode surface. The biosensor has simple operation and excellent analytical performance. The biosensor owns high selectivity and sensitivity with the detection limit of 59.6 fM. Thus, it has broad application prospects in biochemical research. Therefore, the novel ratio probe designed in this paper lays the foundation for developing and applying ratiometric methods in clinical applications and other fields.

CRediT authorship contribution statement

Fa-Ting Xie: Data curation, Formal analysis, Investigation, Methodology. **Xiao-Lan Zhao:** Data curation. **Kuan-Neng Chi:** Data curation, Formal analysis. **Tong Yang:** Conceptualization. **Rong Hu:** Visualization, Formal analysis, Conceptualization, Project administration, Writing - original draft, Writing - review & editing. **Yun-Hui Yang:** Project administration, Supervision, Writing - review & editing.

Declaration of competing interest

The authors declare that they have no known competing financial interests or personal relationships that could have appeared to influence the work reported in this paper.

Acknowledgement

This work is supported by grants awarded by the National Natural Science Foundation of China (Grants No: 21864026 and 21605130) and Natural Science Foundation of Yunnan Province (Grants No: 2018FB016 and 2016FD017).

Appendix A. Supplementary data

Supplementary data to this article can be found online at https://doi.org/10.1016/j.aca.2020.08.007.

References

[1] T.G. Drummond, M.G. Hill, J.K. Barton, Electrochemical DNA sensors, Nat. Biotechnol. 21 (2003) 1192–1199.
[2] D. Li, S. Song, C. Fan, Target-responsive structural switching for nucleic acid-based sensors, Acc. Chem. Res. 43 (2010) 631–641.
[3] C. Fan, K.W. Plaxco, A.J. Heeger, Electrochemical interrogation of conformational changes as a reagentless method for the sequence-specific detection of DNA, Proc. Natl. Acad. Sci. U.S.A. 100 (2003) 9134–9137.
[4] J. Zhang, D. Wang, Y. Li, Ratiometric electrochemical sensors associated with self-cleaning electrodes for simultaneous detection of adrenaline, serotonin, and tryptophan, ACS Appl. Mater. Interfaces 11 (2019) 13557–13563.
[5] C.Y. Deng, X.M. Pi, P. Qian, X.Q. Chen, W.M. Wu, J. Xiang, High-performance ratiometric electrochemical method based on the combination of signal probe and inner reference probe in one hairpin-structured DNA, Anal. Chem. 89 (2017) 966–973.
[6] Y. Du, B.J. Lim, B.L. Li, Y.S. Jiang, J.L. Sessler, A.D. Ellington, Reagentless, Ratiometric electrochemical DNA sensors with improved robustness and reproducibility, Anal. Chem. 86 (2014) 8010–8016.
[7] X.Q. Chen, G.B. Zhou, P. Song, J.J. Wang, J.M. Gao, J.X. Lu, C.H. Fan, X.L. Zuo, Ultrasensitive electrochemical detection of prostate-specific antigen by using antibodies anchored on a DNA nanostructural scaffold, Anal. Chem. 86 (2014) 7337–7342.
[8] M. Qing, S.L. Chen, S.B. Xie, Y. Tang, J. Zhang, R. Yuan, Encapsulation and release of recognition probes based on a rigid three-dimensional DNA "Nanosafe-box" for construction of a electrochemical biosensor, Anal. Chem. 92 (2020) 1811–1817.
[9] Q. Feng, Y. Guo, J. Xu, H. Chen, Self-assembled DNA tetrahedral scaffolds for the construction of electrochemiluminescence biosensor with programmable

DNA cyclic amplification, ACS Appl. Mater. Interfaces 9 (2017) 17637–17644.
[10] L. Zhao, Y. Huang, X. Qi, X. Yan, S. Wang, X. Liang, Nanotetrahedron-assisted electrochemical aptasensor with cooperatively-folding aptamer chimera for sensitive and selective detection of lysozyme in red wines, Anal. Chim. Acta 1095 (2020) 172–178.
[11] Y. Lin, J.P. Jia, R. Yang, D.Z. Chen, J. Wang, F. Luo, L.H. Guo, B. Qiu, Z.Y. Lin, Ratiometric immunosensor for GP73 detection based on the ratios of electrochemiluminescence and electrochemical signal using DNA tetrahedral nanostructure as the carrier of stable reference signal, Anal. Chem. 91 (2019) 3717–3724.
[12] M. Lin, J. Wang, G. Zhou, J. Wang, N. Wu, J. Lu, J. Gao, X. Chen, J. Shi, X. Zuo, C. Fan, Programmable engineering of a biosensing interface with tetrahedral DNA nanostructures for ultrasensitive DNA detection, Angew. Chem. Int. Ed. 54 (2015) 2151–2155.
[13] M. Li, L. Jiao, S. Liu, L. Zhang, H. Li, A new ratiometric electrochemical immunoassay for reliable detection of nuclear matrix protein 22, Anal. Chim. Acta 1086 (2019) 103–109.
[14] X. Zheng, L. Li, L. Zhang, L. Xie, X. Song, J. Yu, Multiple self-cleaning paper-based electrochemical ratiometric biosensor based on the inner reference probe and exonuclease III-assisted signal amplification strategy, Biosens. Bioelectron. 147 (2020) 111769.
[15] L. Hamon, P.L. Llewellyn, T. Devic, A. Ghoufi, G. Clet, V. Guillerm, G.D. Pirngruber, G. Maurin, C. Serre, G. Driver, W. BeeK, E. Jolimaitre, A. Vimont, M. Daturi, G. Férey, Co-adsorption and separation of CO_2-CH_4 mixtures in the highly flexible MIL-53(Cr) MOF, J. Am. Chem. Soc. 131 (2009) 17490–17499.
[16] P. Horcajada, T. Chalati, C. Serre, B. Gillet, C. Sebrie, T. Baati, J.F. Eubank, D. Heurtaux, P. Clayette, C. Kreuz, J. Chang, Y.K. Hwang, V. Marsaud, P. Bories, L. Cynober, S. Gil, G. Férey, P. Couvreur, R. Gref, Porous metal–organic framework nanoscale carriers as a potential platform for drug delivery and imaging, Nat. Mater. 9 (2010) 172–178.
[17] Y. Yang, J. Liu, C. Liang, L. Feng, T. Fu, Z. Dong, Y. Chao, Y. Li, G. Lu, M. Chen, Z. Liu, Nanoscale metal–organic particles with rapid clearance for magnetic resonance imaging-guided photothermal therapy, ACS Nano 10 (2016) 2774–2781.
[18] L. Cui, J. Wu, J. Li, H.X. Ju, Electrochemical sensor for lead cation sensitized with a DNA functionalized porphyrinic metal-organic framework, Anal. Chem. 87 (2015) 10635–10641.
[19] M.H. Teplensky, M. Fantham, P. Li, T.C. Wang, J.P. Mehta, L.J. Young, P.Z. Moghadam, J.T. Hupp, O.K. Farha, C.F. Kaminski, D. Fairen-Jimenez, Temperature treatment of highly porous zirconium-containing metal-organic frameworks extends drug delivery release, J. Am. Chem. Soc. 139 (2017) 7522–7532.
[20] Y. Pan, K. Sun, S. Liu, X. Cao, K. Wu, W.C. Cheong, Z. Chen, Y. Wang, Y. Li, Y. Liu, D. Wang, Q. Peng, C. Chen, Y. Li, Core-shell ZIF-8@ZIF-67-derived CoP nanoparticle-embedded N-doped carbon nanotube hollow polyhedron for efficient overall water splitting, J. Am. Chem. Soc. 140 (2018) 2610–2618.
[21] T.Z. Liu, R. Hu, X. Zhang, K.L. Zhang, Y. Liu, X.B. Zhang, R.Y. Bai, D.L. Li, Y.H. Yang, Metal-organic framework nanomaterials as novel signal probes for electron transfer mediated ultrasensitive electrochemical immunoassay, Anal. Chem. 88 (2016) 12516–12523.
[22] A. Gosai, B.S.H. Yeah, M. Nilsen-Hamilton, P. Shrotriya, Label free thrombin detection in presence of high concentration of albumin using an aptamer-functionalized nanoporous membrane, Biosens. Bioelectron. 126 (2019) 88–95.
[23] S.R. Coughlin, Thrombin signaling and protease-activated receptors, Nature 407 (2000) 258–264.
[24] L. Martorell, J. Martínez-González, C. Rodríguez, M. Gentile, O. Calvayrac, L. Badimon, Thrombin and protease-activated receptors (PARs) in atherothrombosis, Thromb. Haemostasis 99 (2008) 305–315.
[25] H. Wang, G. Reiser, Thrombin signaling in the brain: the tole of protease-activated receptors, Biol. Chem. 384 (2005) 193–202.
[26] C. Tuerk, L. Gold, Systematic evolution of ligands by exponential enrichment: RNA ligands to bacteriophage T4 DNA polymerase, Science 249 (1990) 505–510.
[27] A.D. Ellington, J.W. Szostak, In vitro selection of RNA molecules that bind specific ligands, Nature 346 (1990) 818–822.
[28] R. Hu, X. Zhang, Q. Xu, D. Lu, Y. Yang, Q. Xu, Q. Ruan, L. Mo, X. Zhang, A universal aptameric biosensor: multiplexed detection of small analytes via aggregated perylene-based broad-spectrum quencher, Biosens. Bioelectron. 92 (2017) 40–46.
[29] X. Zhang, K. Chi, D. Li, Y. Deng, Y. Ma, Q. Xu, R. Hu, Y. Yang, 2D-porphrinic covalent organic framework-based aptasensor with enhanced photoelectrochemical response for the detection of C-reactive protein, Biosens. Bioelectron. 129 (2019) 64–71.
[30] J. Li, C. Fan, H. Pei, J. Shi, Q. Huang, Smart drug delivery nanocarriers with self-assembled DNA nanostructures, Adv. Mater. 25 (2013) 4386–4396.
[31] M.F. Huang, Y.C. Kuo, C. Huang, H. Chang, Separation of long double-stranded DNA by nanoparticle-filled capillary electrophoresis, Anal. Chem. 76 (2004) 192–196.
[32] S.S.Y. Chui, S.M.F. Lo, J.P.H. Charmant, A.G. Orpen, L.D. Williams, A chemically functionalizable nanoporous material $[Cu_3(TMA)_2(H_2O)_3]_n$, Science 283 (1999) 1148–1150.
[33] D. Li, X. Zhang, Y. Ma, Y. Deng, R. Hu, Y. Yang, Preparation of an OTA aptasensor based on a metal–organic framework, Anal. Methods 10 (2018) 3273–3279.
[34] K.M.L. Taylor-Pashow, J.D. Rocca, Z. Xie, S. Tran, W. Lin, Postsynthetic modifications of iron-carboxylate nanoscale metal-organic frameworks for imaging and drug delivery, J. Am. Chem. Soc. 131 (40) (2009) 14261–14263.
[35] P. Chen, T. Xiao, Y. Qian, S. Li, S. Yu, A nitrogen-doped graphene/carbon nanotube nanocomposite with synergistically enhanced electrochemical activity, Adv. Mater. 25 (2013) 3192–3196.
[36] G. López, D. Castner, B. Ratner, XPS O 1s binding energies for polymers containing hydroxyl, ether, ketone and ester groups, Surf. Interface Anal. 17 (1991) 267–272.
[37] Y. Hou, Z. Wen, S. Cui, X. Guo, J. Chen, Constructing 2D porous graphitic C_3N_4 nanosheets/nitrogen-doped graphene/layered MoS_2 ternary nanojunction with enhanced photoelectrochemical activity, Adv. Mater. 25 (2013) 6291–6297.
[38] A.P. Grosvenor, B.A. Kobe, M.C. Biesinger, N.S. McIntyre, Investigation of multiplet splitting of Fe 2p XPS spectra and bonding in iron compounds, Surf. Interface Anal. 36 (2004) 1564–1574.
[39] X. Lu, Y. Jin, X. Zhang, G. Xu, D. Wu, J. Lv, Y. Wu, Controllable synthesis of graphitic C_3N_4/ultrathin MoS_2 nanosheet hybrid nanostructures with enhanced photocatalytic performance, Dalton Trans. 45 (2016) 15406–15414.
[40] Y. Zhang, Y. Shen, J. Yuan, D. Han, Z. Wang, Q. Zhang, L. Niu, Design and synthesis of multifunctional materials based on an ionic-liquid backbone, Angew. Chem. Int. Ed. 45 (2006) 5867–5870.
[41] Q. Zhang, G. Fan, W. Chen, Q. Liu, X. Zhang, X. Zhang, Q. Liu, Electrochemical sandwich-type thrombin aptasensor based on dual signal amplification strategy of silver nanowires and hollow Au–CeO_2, Biosens. Bioelectron. 150 (2020) 111846.
[42] Z. Chen, L. Tan, L. Hu, Y. Zhang, S. Wang, F. Lv, Real Colorimetric thrombin aptasensor by masking surfaces of catalytically active gold nanoparticles, ACS Appl. Mater. Interfaces 8 (2016) 102–108.
[43] J.M. Yang, B.T. Dou, R. Yuan, Y. Xiang, Aptamer/protein proximity binding-triggered molecular machine for amplified electrochemical sensing of thrombin, Anal. Chem. 89 (2017) 5138–5143.
[44] X. Li, Y. Wu, J. Niu, D. Jiang, D. Xiao, C. Zhou, One-step sensitive thrombin detection based on a nanofibrous sensing platform, J. Mater. Chem. B. 7 (2019) 5161–5169.
[45] T. Yu, D. Wei, Z. Li, L. Pan, Z. Zhang, Z. Tian, Z. Liu, Target-modulated sensitization of upconversion luminescence by NIR-emissive quantum dots: a new strategy to construct upconversion biosensors, Chem. Commun. 56 (2020) 1976–1979.
[46] T. Fan, Y. Du, Y. Yao, J. Wu, S. Meng, J. Luo, X. Zhang, D. Yang, C. Wang, Y. Qian, F. Gao, Rolling circle amplification triggered poly adenine-gold nanoparticles production for label-free electrochemical detection of thrombin, Sensor. Actuator. B Chem. 266 (2018) 9–18.